Crystallization of poly(3-hydroxybutyrate) by exfoliated graphite nanoplatelets

ARTICLE *in* JOURNAL OF APPLIED POLYMER SCIENCE · NOVEMBER 2007

Impact Factor: 1.77 · DOI: 10.1002/app.25137

4 AUTHORS:

Dana Miloaga
PPG Industries
6 PUBLICATIONS **30** CITATIONS
SEE PROFILE

Hazel-Ann Hosein
CYTEC Industries
22 PUBLICATIONS **320** CITATIONS
SEE PROFILE

Manjusri Misra
University of Guelph
472 PUBLICATIONS **9,626** CITATIONS
SEE PROFILE

Lawrence T Drzal
Michigan State University
422 PUBLICATIONS **12,829** CITATIONS
SEE PROFILE

Crystallization of Poly(3-hydroxybutyrate) by Exfoliated Graphite Nanoplatelets

Dana G. Miloaga, Hazel-Ann A. Hosein, Manjusri Misra, Lawrence T. Drzal

Composite Materials and Structures Center, Michigan State University, East Lansing, Michigan 48824

Received 7 March 2006; accepted 9 July 2006
DOI 10.1002/app.25137
Published online 30 July 2007 in Wiley InterScience (www.interscience.wiley.com).

ABSTRACT: Poly(3-hydroxybutyrate) (PHB) has been shown to be efficiently nucleated by exfoliated graphite nanoplatelets (xGnP). The nucleating effect of xGnP was investigated using differential scanning calorimetry, optical microscopy and atomic force microscopy. Nonisothermal crystallization of PHB from the melt required lower activation energies for PHB containing 1 wt % and 3 wt % xGnP (−214 and −102 kJ/mol respectively) than for pure PHB (−60 kJ/mol). A kinetic study of the PHB/xGnP crystallization employing a modified form of the Avrami equation revealed that the presence of xGnP increased the PHB crystallization temperature, as well as the crystallization rates, and generated smaller and more numerous spherulites. Optical microscopy and atomic force microscopy confirmed the incorporation of xGnP into the lamellar structure of the PHB spherulites and provided insight into the influence of xGnP on spherulite size and lamellae thickness. © 2007 Wiley Periodicals, Inc. J Appl Polym Sci 106: 2548–2558, 2007

Key words: poly(3-hydroxybutyrate); expanded graphite nanoplatelets nonisothermal crystallization; nucleation; morphology

INTRODUCTION

The United States generates more than 14 million tons of plastic waste annually,[1] of which only 28% is recycled[2] at a cost of several million dollars.[3] In an effort to reduce the amount of plastic waste generated, ''green'' researchers have turned their attention to biodegradable polymers as potential alternatives to traditionally used materials like polyethylene terephthalate and polyolefins.[4] Biodegradable polymers obtained from biologically based feedstocks are especially attractive since these reduce our reliance on polymers derived from depleting natural resources such as petroleum. One group of biodegradable polymers that has received considerable attention is the poly(hydroxyalkanoates) (PHAs),[5,6] which are thermoplastic biopolyesters typically synthesized by various bacteria and microorganisms that use them as reserves of carbon and energy.[5–7] Materials produced from PHAs can be totally biodegraded under aerobic and/or anaerobic conditions[5–10] at the end of their lifetimes.

One of the most investigated PHAs is poly (hydroxybutyrate) (PHB), which, besides being biodegradable and biocompatible, is attractive due to its availability, processibility, and mechanical and barrier properties comparable to isotactic polypropylene and other synthetic polymers.[11,12] PHB is also a highly crystalline thermoplastic that can be extruded, injection molded, and spun[13,14] into fibers without modification of traditional polymer processing equipment. PHB also has a low elongation at break (less than 10%), an impact strength of 3 kJ/mm^2, a modulus (1.7 GPa), and a fracture stress of 35 MPa.[15] Despite having these desirable characteristics, PHB is not widely applied in the manufacturing industry, primarily due to its narrow processibility window (PHB melts around 180°C,[8] very close to its thermal degradation temperature), and to its brittleness which is related to its crystallization behavior. A host of researchers has attempted to resolve these processibility issues by copolymerizing PHB with other hydroxyalkanoates,[7,16,17] mainly hydroxyvalerate and hydroxyhexanoate, blending with poly(ethylene oxide), poly(vinyl alcohol), or poly(lactide), for example,[18–23] adding plasticizers like citric esters[24] and processing aids,[15] and/or through annealing.[25]

The brittleness of PHB[15,25–28] is known to stem from three factors: a glass transition temperature close to room temperature, secondary crystallization occurring upon storage at room temperature, and extremely low nucleation density. All these factors are interrelated, and derive from the high purity of PHB and from its stereochemical regularity.[26] Detailed studies of the crystallization phenomena occurring in bacterial PHB[26,29] outline the importance of physical aging as an intrinsic property of this poly-

Correspondence to: L.T. Drzal (drzal@egr.msu.edu).
Contract grant sponsor: US Environmental Protection Agency (EPA) Science; contract grant number: RD 8309040.

mer, attributed to progressive crystallization occurring upon storage at room temperature. As a result of its biosynthetic preparation, solvent-based extraction and purification processes, PHB is exceptionally pure and has a very low level of heterogeneous nuclei that could initiate crystallization.[27] Because of its low nucleation density, when cooled from the melt state, PHB forms large spherulitic structures that continue growing into each other during storage, and are prone to cracking, resulting in materials with low impact resistance and high brittleness.

There is an ongoing research thrust to discover efficient nucleating agents for PHB and its copolymers. Efficient nucleating agents would increase the polymer's crystallization temperature, increase the crystallization rates, and generate smaller and more numerous spherulites, leading to materials with increased mechanical properties. Compounds ranging from talc,[30–32] boron nitride,[31–33] terbium oxide,[32] lanthanum oxide,[32] saccharin,[33,34] phtalimide,[33] cyclodextrin,[30] and lignin[35] were investigated as possible nucleating agents for PHB and several nucleation mechanisms were proposed.[31,34–36] Among the nucleating agents mentioned earlier, micro- and nanosized inorganic particles were shown to have the added advantage of acting as reinforcements for the polymer. For example, clay nanoparticles, commonly used as reinforcements for thermoplastic polymers,[37,38] were proven to efficiently nucleate and to reinforce PHB[39] and poly(3-hydroxybutyrate-*co*-3-hydroxyvalerate).[40] Also, single-walled carbon nanotubes were shown to nucleate polypropylene[41] and to affect the thermal properties and the morphology of poly (hydroxybutyrate-*co*-hydroxyvalerate).[42]

We report here on the nucleating effect of exfoliated graphite nanoplatelets (xGnP) on PHB. Graphite has a similar structure to boron nitride, and can be intercalated and exfoliated into very thin nanosized platelets[43] with extremely high surface area and in-plane stiffness as high as 1060 GPa.[44] The nonisothermal crystallization of PHB from the melt was examined, since a fundamental understanding is essential for optimizing the processing conditions for thermoplastic materials under dynamic conditions like extrusion and injection molding.[29,45–47] A kinetic analysis of the nonisothermal crystallization from melt was undertaken using models based on modifications of the Avrami equation. Optical microscopy and atomic force microscopy (AFM) were used to characterize the morphologies of PHB/xGnP systems and to offer further information on the crystallization process.[48–50] AFM is now routinely used to study the surface morphology and nanostructure of crystalline polymers and polymer composites,[51–53] offering insights into processes such as crystallization, crystal thickening, and crystal deformation, phenomena which can also be observed *in situ*.[51]

EXPERIMENTAL

Materials

Poly(hydroxybutyrate) was obtained from Metabolix (Cambridge, MA), and used without further purification. The exfoliated graphite nanoplatelets having an average size of 1 μm (xGnP-1) was produced in-house[43,54] starting from GraphGuard™ 160-50A acid intercalated graphite produced by Graftech (Cleveland, OH). The xGnP has a surface area of $\sim 100\ m^2/g$ and consists of platelets $\sim$ 10 nm in thickness and 1 μm in diameter. The platelet basal plane is a graphene sheet, uniform in structure and surface energy, with evidence of some oxygen functionalities located at the edges of these basal surfaces.

Sample preparation

Samples of pure PHB and PHB containing, 0.01, 1, and 3 wt % xGnP-1 were prepared by extrusion and injection molding. The PHB powder, previously dried in a vacuum oven at 80°C for 3 h to remove the moisture, was mixed with the xGnP-1 and extruded using a DSM microextruder (15 cm^3 capacity) (DSM Research B.V., The Nederlands). The temperatures in the three heating zones of the microextruder were 175, 185, and 195°C respectively. The mixtures were extruded at 100 rpm, and the cycle time was 3 min. The extruded polymer systems were injection molded at a fixed temperature of 50°C.

Methods

Thermal analysis: differential scanning calorimetry

The melting and crystallization behavior of PHB/xGnP-1 samples were investigated using a 2920 Modulated DSC (TA Instruments). The runs were performed under nitrogen flow, after calibrating the DSC instrument using an Indium standard. For each run, a fresh sample (5–10 mg) of polymer was heated from room temperature to 190°C, kept isothermal for 5 min (to remove the thermal history), then cooled to −60°C, reheated to 190°C, and cooled to room temperature. Six different heating/cooling rates were used: 5, 8, 10, 14, 17, and 20°C/min, and the data recorded during the second cooling step were analyzed. During the nonisothermal crystallization of PHB study, the samples were run consecutively, using the same sealed aluminum pan as control to reduce error.

Optical microscopy

The samples for optical microscopy (OM) were prepared as thin polymer films by heating very thin sections of PHB/xGnP-1 injection molded bars in a Mettler Toledo FP82 hot stage. The polymer was

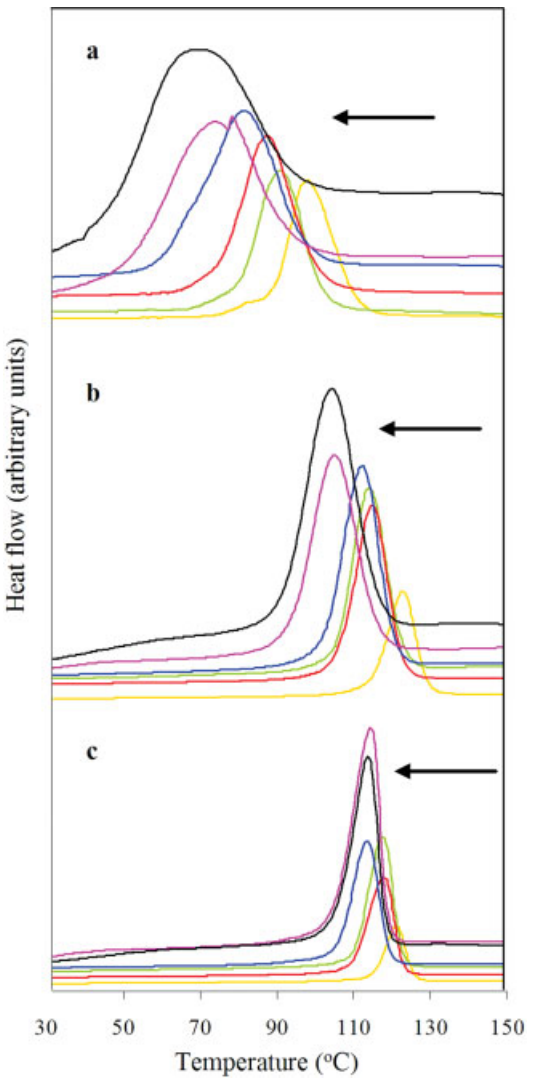

Figure 1 Nonisothermal crystallization curves obtained for (a) pure PHB, (b) PHB/1% xGnP-1 and (c) PHB/3% xGnP-1 at six cooling rates: − 5°C/min; −8°C/min; −10°C/min; −14°C/min; −17°C/min; and −20°C/min respectively. (The arrows indicate increasing cooling rates.) [Color figure can be viewed in the online issue, which is available at www.interscience.wiley.com.]

placed on glass or mica slides, covered with glass or mica cover slips, and heated at a rate of 20°C/min from room temperature to 190°C, kept isothermal for 3 min, then either allowed to crystallize upon cooling to room temperature or to crystallize isothermally at different preset crystallization temperatures. The morphology of PHB and the size of the spherulites were observed using an Olympus BH2 optical microscope equipped with a Spot™ camera.

Atomic force microscopy

Thin polymer films were prepared as described for optical microscope, using the Mettler Toledo FP80 hot stage. All images were collected on a Nanoscope™ IV instrument (Veeco, Santa Barbara, CA) equipped with a *J* scanner. Images were collected in either contact or tapping mode, using commercially available silicon or silicon nitride cantilevers. The AFM was initially calibrated by the manufacturer but because of the nonlinear electrical response of piezo materials, the electrical signals applied to SPM scanners were periodically calibrated to ensure accuracy. Calibration standards, e.g., the TGZ01 standard (MikroMasch, CA) were imaged to ensure that the pitch and *z* distances are in agreement with those specified by the manufacturer. Images were typically collected at a scan rate of 0.5 Hz for scans sizes larger than 5 × 5 μm^2 and up to 1 Hz for scan sizes less than 1 × 1 μm^2. Some of the images were first-order flattened and scan lines were erased.

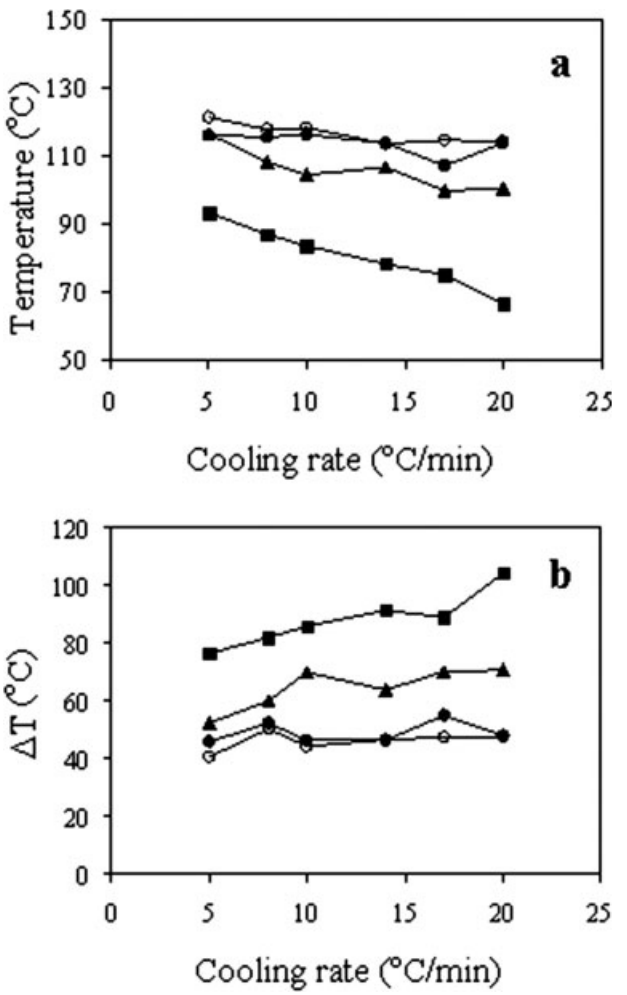

Figure 2 Graphs showing (a) the crystallization temperatures and (b) the degrees of supercooling versus cooling rate for pure PHB (■), PHB/0.01% xGnP-1 (○), PHB/1% xGnP-1 (●), and PHB/3% xGnP-1 (▲).

TABLE I
Summary of Modified Avrami Analysis Results for the Nonisothermal Crystallization of PHB, PHB/1% xGnP-1, and PHB/3% xGnP-1

D (°C/min)	T_0 (°C)	T_p (°C)	T_∞ (°C)	T_m (°C)	ΔT (°C)	t_{max} (min)	$t_{1/2}$ (min)	n	log ($-Z$)	Z	log ($-Z_c$)	Z_c
PHB												
5	109.00	93.14	74.35	174.44	81.30	6.89	3.33	1.8539	2.3162	−10.1371	−2.0274	0.1317
8	105.47	86.64	63.26	174.15	87.51	5.24	2.55	2.3035	3.0944	−22.0740	−2.7592	0.0633
10	106.99	83.41	62.64	173.80	90.39	4.41	2.48	2.3837	3.2070	−24.7049	−2.4705	0.0845
14	101.88	78.04	56.47	173.42	95.38	3.22	1.78	2.0240	2.9787	−19.6622	−1.4044	0.2455
17	100.84	74.95	51.07	174.42	99.47	2.91	1.55	1.9675	2.8900	−17.9933	−1.0584	0.3470
20	101.33	66.21	47.99	173.33	107.12	2.72	1.49	2.8361	1.9022	−6.7006	−0.3350	0.7153
PHB+1% xGnP-1												
5	129	116.13	105	161.6	45.47	4.70	1.85	0.4208	−1.4825	−0.2271	−0.0454	0.9556
8	127	108.04	99	167.8	59.76	3.90	1.58	0.3856	−0.9347	−0.3927	−0.0491	0.9521
10	128	104.17	96	162.3	58.13	3.19	1.24	0.3471	−1.6324	−0.1955	−0.0195	0.9806
14	124	106.39	88	160.02	53.63	2.52	0.9	0.4119	−1.7802	−0.1686	−0.0120	0.9880
17	121	99.64	90	162	62.36	1.58	0.73	0.3946	−1.9053	−0.1488	−0.0088	0.9913
20	123	100.16	88	161.64	61.48	1.72	0.6	0.4184	−1.9518	−0.1420	−0.0071	0.9929
PHB+3% xGnP-1												
5	128.66	116.13	100.07	168.6	52.47	5.68	2.77	0.3698	−1.3043	−0.2714	−0.0543	0.9472
8	121.63	108.04	93.116	168	59.96	3.54	1.95	0.4291	−1.4995	−0.2232	−0.0279	0.9725
10	119.99	104.17	84.628	174.17	70	3.49	1.8	0.3948	−1.5104	−0.2208	−0.0221	0.9782
14	119.07	106.39	89.468	170.39	64	2.10	1.07	0.4443	−1.7528	−0.1733	−0.0124	0.9877
17	114.37	99.64	84.209	169.91	70.27	1.76	0.99	0.5130	−1.7894	−0.1671	−0.0098	0.9902
20	112.73	100.16	83.936	170.79	70.63	1.43	0.81	0.5732	−1.8840	−0.1520	−0.0076	0.9924

RESULTS AND DISCUSSION

Crystallization of PHB in the presence of xGnP-1

The nonisothermal crystallization of pure PHB and PHB containing 1wt %, and 3 wt % xGnP-1 from the melt was studied using differential scanning calorimetry. The melting temperature (T_m), the onset and end of crystallization temperatures (T_0 and T_∞), the temperature of the crystallization peak (T_p), the enthalpies of fusion and the crystallization enthalpies (ΔH_f and ΔH_c) were recorded for heating/cooling at six different rates ($D = 5$, 8, 10, 14, 17, and 20°C/min, respectively). Figure 1 shows the nonisothermal crystallization curves for the PHB/xGnP-1 systems described earlier. After the addition of xGnP-1, the crystallization peaks shifted to higher temperatures, which was the first indication of the nucleating effect ox xGnP-1. The crystallization peaks also became narrower, which suggested that PHB spherulites formed in the presence of xGnP-1 were smaller than the spherulites formed by the neat polymer.[42] Figure 2(a) and Table I summarize the values of T_p recorded for PHB containing different concentrations of xGnP-1, at different cooling rates. Figure 2(b) and Table I show that for PHB/xGnP-1 systems the degrees of supercooling (defined as the difference between the melting temperature and the temperature of the crystallization peak, $\Delta T = T_m - T_p$) were lower than that for pure PHB. The nucleating effect of graphite nanoplatelets was more evident at lower concentrations. Both the shifts of the crystallization peaks and the decreases of the degree of supercooling are evidence of the nucleating effect of xGnP-1.

Kinetic analysis of the nonisothermal crystallization from melt

Based on the shifts of T_p, the narrowing of the crystallization peaks, and the decrease of the degree of supercooling of PHB after the addition of xGnP-1, it was concluded that PHB crystallizes faster in the presence of xGnP-1. To verify this, a kinetic analysis was performed to compare the crystallization rates of the various PHB/xGnP-1 systems. Most methods used for describing nonisothermal crystallization are based on modifications of Avrami eq. (1),[41,45–47,55–58] which accurately describes isothermal crystallization of polymers:

$$1 - X_t = \exp(-Z_t^n), \quad (1)$$

where X_t is the relative degree of crystallinity, Z is an overall rate constant characterizing both nucleation and growth contributions, and n is a mechanism constant whose value depends on the type of nucleation and growth process parameters.[46] A modification proposed by Jeziorny,[58] and applied to PHB,[29] successfully described the kinetics of nonisothermal crystallization of PHB/xGnP-1 samples. The cooling rate (D), assumed to be constant, was the factor used in correcting the rate constant, Z:

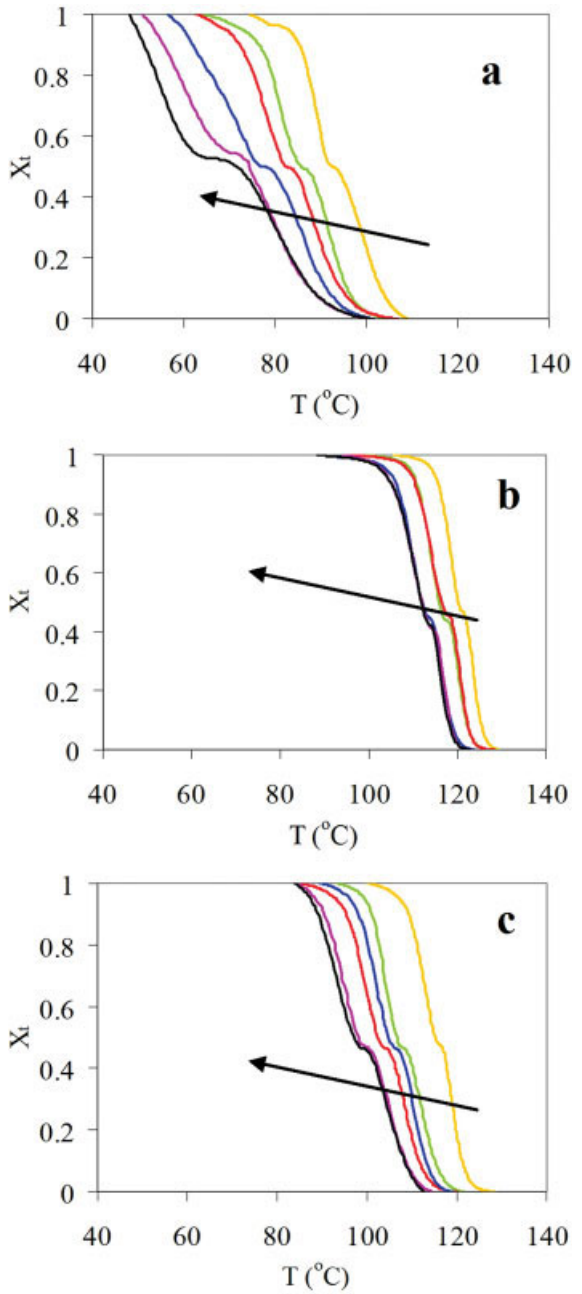

Figure 3 Development of relative crystallinity with temperature for (a) pure PHB, (b) PHB/1% xGnP-1, (c) PHB/3% xGnP-1 at six cooling rates: −5°C/min; −8°C/min; −10°C/min; −14°C/min; −17°C/min; and −20°C/min, respectively. (The arrows indicate increasing cooling rates.) [Color figure can be viewed in the online issue, which is available at www.interscience.wiley.com.]

$$\log Z_c = \frac{\log Z}{D} \tag{2}$$

The relative degree of crystallinity, X_t, and the absolute degree of crystallinity at each crystallization temperature, X_c, were determined as follows:

$$X_c = \frac{\int_{T_0}^{T} \left(\frac{dH_c}{dT}\right) dT}{(1 - w_{\text{xGnP}-1})\, \Delta H_f^0}, \tag{3}$$

$$X_t = \frac{\int_{T_0}^{T} \left(\frac{dH_c}{dT}\right) dT}{\int_{T_0}^{T_\infty} \left(\frac{dH_c}{dT}\right) dT}, \tag{4}$$

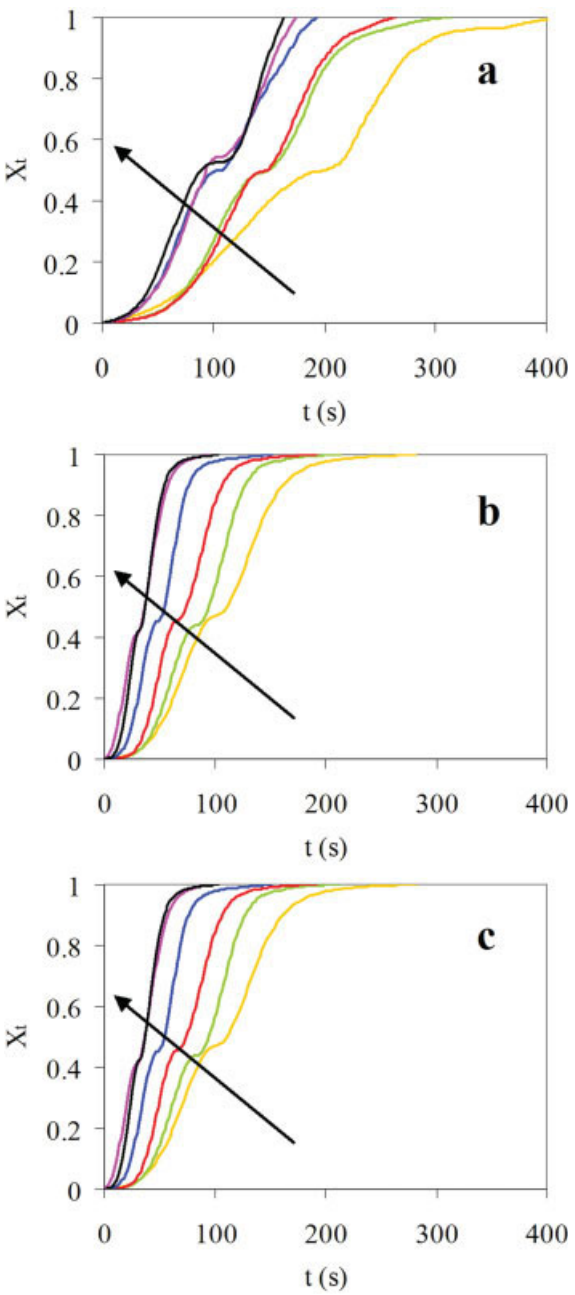

Figure 4 Development of relative crystallinity with time for (a) pure PHB, (b) PHB/1% xGnP-1, (c) PHB/3% xGnP-1 at six cooling rates: −5°C/min; −8°C/min; −10°C/min; −14°C/min; −17°C/min; and −20°C/min respectively. (The arrows indicate increasing cooling rates.) [Color figure can be viewed in the online issue, which is available at www.interscience.wiley.com.]

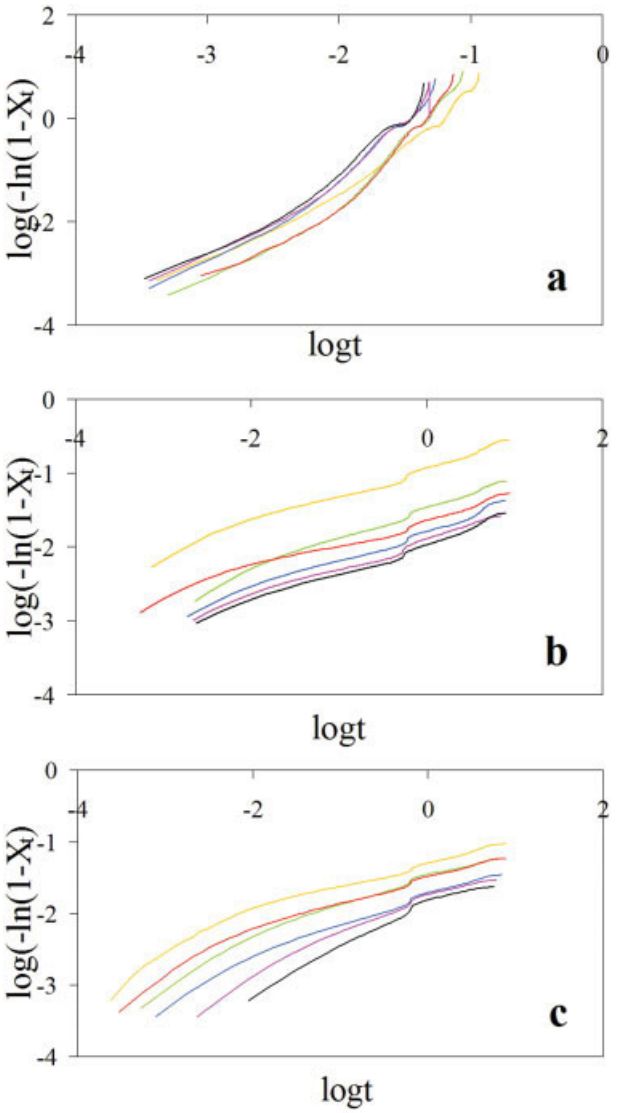

Figure 5 Graphs showing the results of modified Avrami analysis for (a) PHB, (b) PHB/1% xGnP-1, and (c) PHB/3% xGnP-1 at six cooling rates: −5°C/min; −8°C/min; −10°C/min; −14°C/min; −17°C/min; and −20°C/min. [Color figure can be viewed in the online issue, which is available at www.interscience.wiley.com.]

where $w_{xGnP\text{-}1}$ is the mass fraction of xGnP-1 in the polymer system, $\Delta H_f^0 = 146$ J/g is the thermodynamic melting enthalpy of 100% pure crystalline PHB,[18] and ΔH_c is the crystallization enthalpy recorded by DSC.

The development of relative crystallinity with temperature for the PHB/xGnP-1 systems investigated is presented in Figure 3. In each of the three cases, after adding xGnP-1 to PHB, complete crystallization was achieved over a narrower temperature range, and also in a shorter time. (Fig. 4) The *S*-shaped curves indicate that pure PHB crystallizes in two steps, and this phenomenon, also observed for ethylene terephtalate–ethylene oxide segmented copolymers,[46] is explained in terms of an initial fast growth phase of the crystals in an amorphous environment, followed by a slower growth phase as the crystals

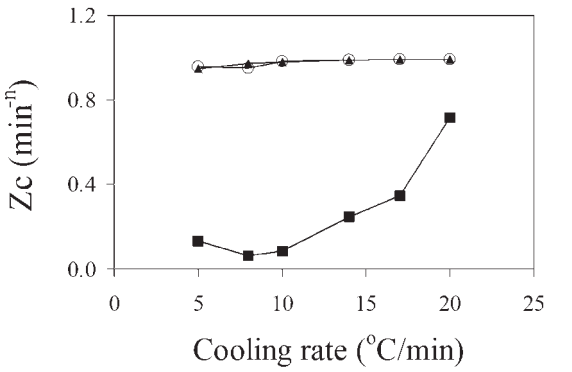

Figure 6 Nonisothermal crystallization rate parameters for PHB/xGn-1 systems, determined according to modified Avrami analysis.

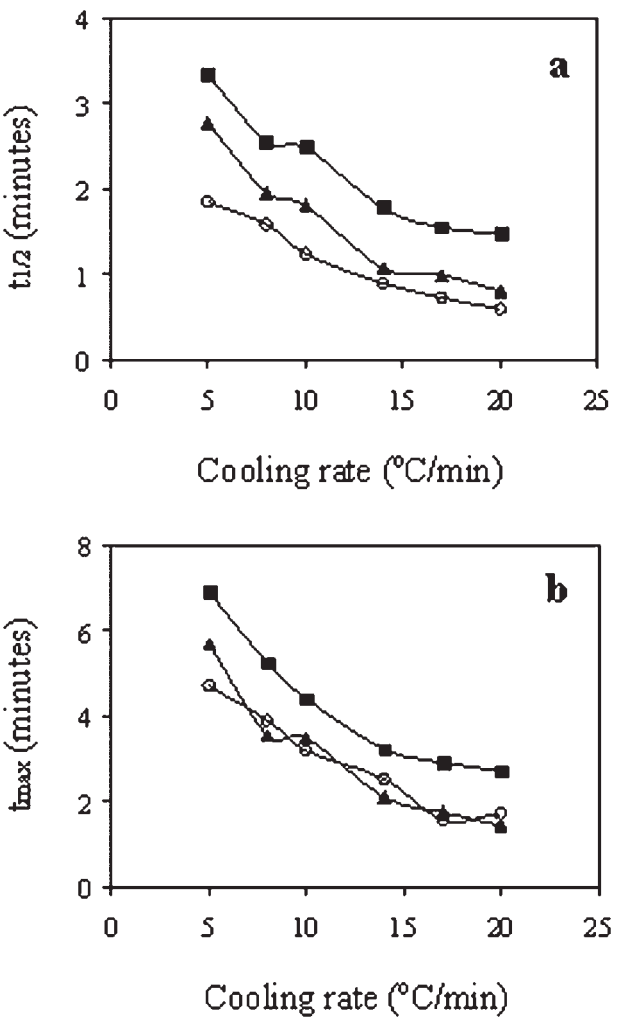

Figure 7 Graphs showing (a) the half-time crystallization times and (b) the maximum crystallization times for pure PHB (■),PHB/1% xGnP-1 (○), and PHB/3% xGnP-1 (▲), determined according to modified Avrami analysis.

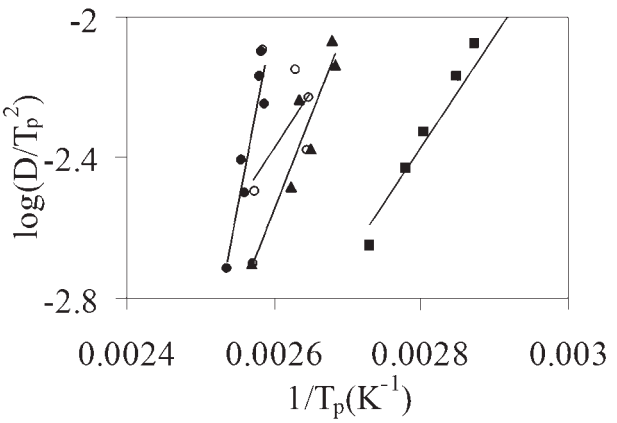

Figure 8 Kissinger plots used for determining the activation energy for nonisothermal crystallization of pure PHB (■), PHB/0.01% xGnP-1 (○), PHB/1% xGnP-1 (●), and PHB/3% xGnP-1 (▲).

begin to impinge on each other in the interlamellar region.

The kinetic parameters for the nonisothermal crystallization PHB/xGnP-1 samples were determined by plotting log [−ln (1 − X_t) versus log t (Fig. 5). For pure PHB, and PHB containing 1 and 3 wt % xGnP-1, the curves were linear at first and then deviated from linearity, due to secondary crystallization.[45] However, for systems containing 0.01 wt % xGnP-1, the plots were not linear, possibly due to nonuniform dispersion of xGnP-1 in PHB, a result of poor mixing in the microextruder. Hence, these samples were not further subjected to kinetic analysis. The values of the kinetic parameters n, Z, and Z_c for neat PHB, and for PHB containing 1 and 3 wt % xGnP-1 were obtained from the slopes and intercepts of the lines in Figure 5, and are summarized in Table I. According to the modified Avrami analysis, the rate of crystallization of pure PHB increased with increasing cooling rate (Fig. 6). For PHB samples containing 1 and 3 wt % xGnP-1, the crystallization rate parameters were higher than for pure PHB, but were independent of the cooling rate. Our results furthermore show that the time required to achieve half of the final crystallinity ($t_{1/2}$), as well as the maximum crystallization time, were higher for pure PHB than for PHB containing expanded graphite nanoplatelets (Fig. 7(a,b), and Table I).

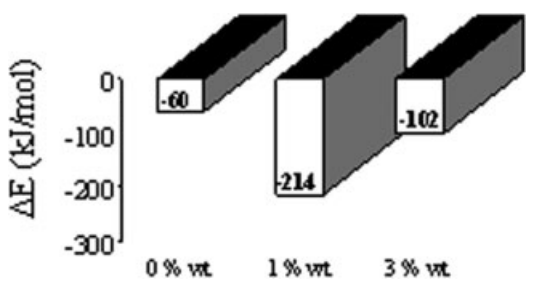

Figure 9 Activation energies for the nonisothermal crystallization from melt of PHB/xGnP-1 systems.

The activation energies for the nonisothermal crystallization from melt were determined using the Kissinger method,[45,59] based on the peak temperatures recorded by DSC for different cooling rates (Table I):

$$\frac{d\left(\ln\left(\frac{D}{T_p}\right)\right)}{d\left(\frac{1}{T_p}\right)} = -\frac{\Delta E}{R}, \tag{5}$$

where R is the universal gas constant, ΔE is the activation energy, and the other parameters are as defined previously. The activation energies were calculated using the slopes of the lines obtained by plotting $\log(D/T_p^2)$ versus $1/T_p$ (Fig. 8, and Table I). For PHB, PHB/1 wt % xGnP-1, and PHB/3 wt % xGnP-1, the activation energies were found to be −60.41 kJ/mol, −213.61 kJ/mol, and −101.86 kJ/mol, respectively, (Fig. 9). ΔE for the nonisothermal crystallization from melt of PHB was in agreement with the value of −64.6 kJ/mol reported by An et al.[29]

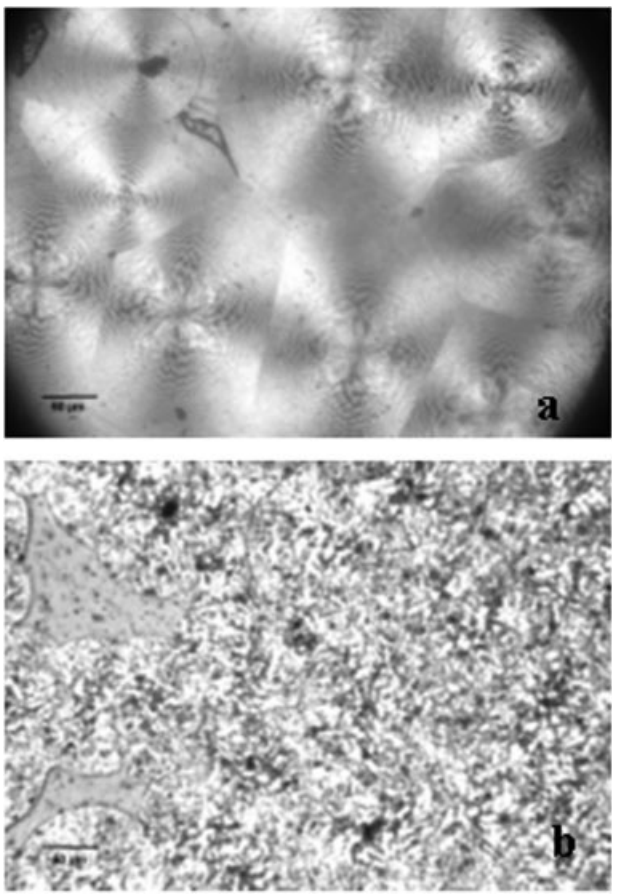

Figure 10 Optical micrographs showing spherulites of (a) pure PHB and (b) PHB/0.01 wt % xGnP-1 formed during nonisothermal crystallization from the melt.

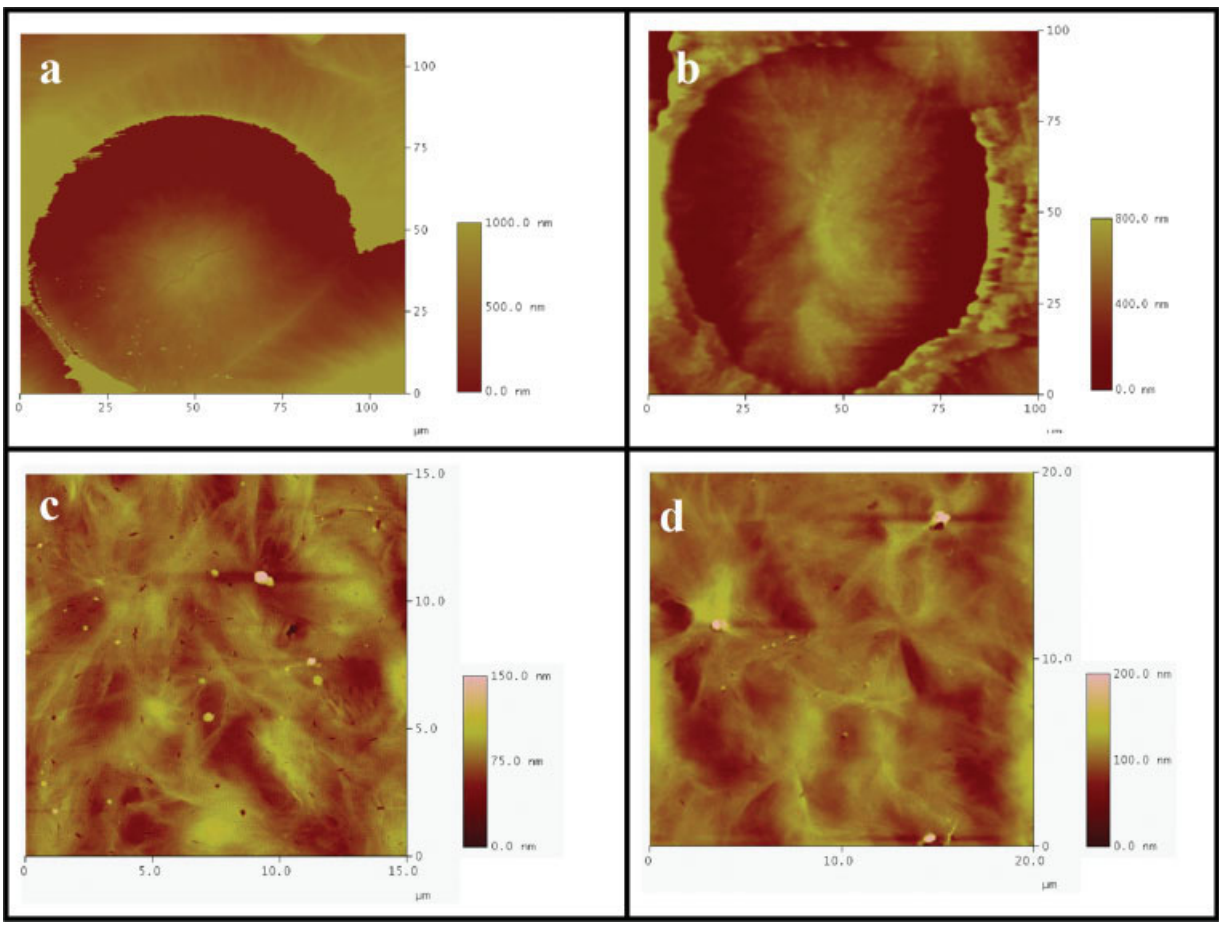

Figure 11 AFM tapping mode height images (top view) showing spherulites of (a) pure PHB and PHB containing, (b) 0.01 wt % xGnP, (c) 1 wt % xGnP and (d) 3 wt % xGnP. [Color figure can be viewed in the online issue, which is available at www.interscience.wiley.com.]

Morphology of PHB/xGnP-1 systems

Optical microscopy was used to observe the distribution and growth of the crystallites formed by pure PHB and PHB/xGnP-1 systems during nonisothermal cooling from the melt, and their morphologies after crystallization. As shown in Figure 10(a), pure PHB formed large, well-defined banded spherulitic structures having an average radius of 70 μm. The optical micrographs obtained for PHB/1 wt % xGnP-1 and PHB/3 wt % xGnP-1 (not shown) showed agglomerations of numerous, small spherulites, which crystallized spontaneously from the melt. This result was not unexpected since the high concentration of xGnP-1 added (1 and 3 wt %) introduced many heterogeneous nuclei, which initiated nucleation of the PHB at 110–113°C. In an attempt to observe the crystallization of PHB in the presence of xGnP-1, PHB samples containing 0.01 wt % xGnP-1 were prepared. The addition of a lower concentration of xGnP-1 to PHB led to the formation of spherulites now large enough to be observed with optical microscopy [Fig. 10(b)].

Atomic force microscopy was employed to provide further details regarding the sizes of the spherulites and topographical information. AFM images were collected for the pure PHB, and PHB containing 0.01, 1, and 3 wt % xGnP-1 (Fig. 11). Figure 11(a) shows an AFM height image of a PHB spherulite formed upon nonisothermal crystallization of PHB from the melt, having an approximate diameter of 90 μm, which is most likely an overestimation due to tip convolution effects. Figure 11(b) shows an AFM height image for a spherulite formed from the PHB/0.01 wt % xGnP-1 system also having a diameter of about 90 μm. In the case of the PHB/xGnP-1 systems having higher concentrations of graphite nanoplatelets, the crystallites formed appeared to be much smaller and impinged into each other [Fig. 11(b, c)], so despite the accuracy of AFM, due to the nature of the sample, it was difficult to determine the exact sizes of the spherulites.

These AFM results indicate that the lamellar thickness of pure PHB spherulites crystallized from the melt ranges from 7 to 20 nm, as shown in the cross-sectional analysis in Figure 12(a). The lamellar struc-

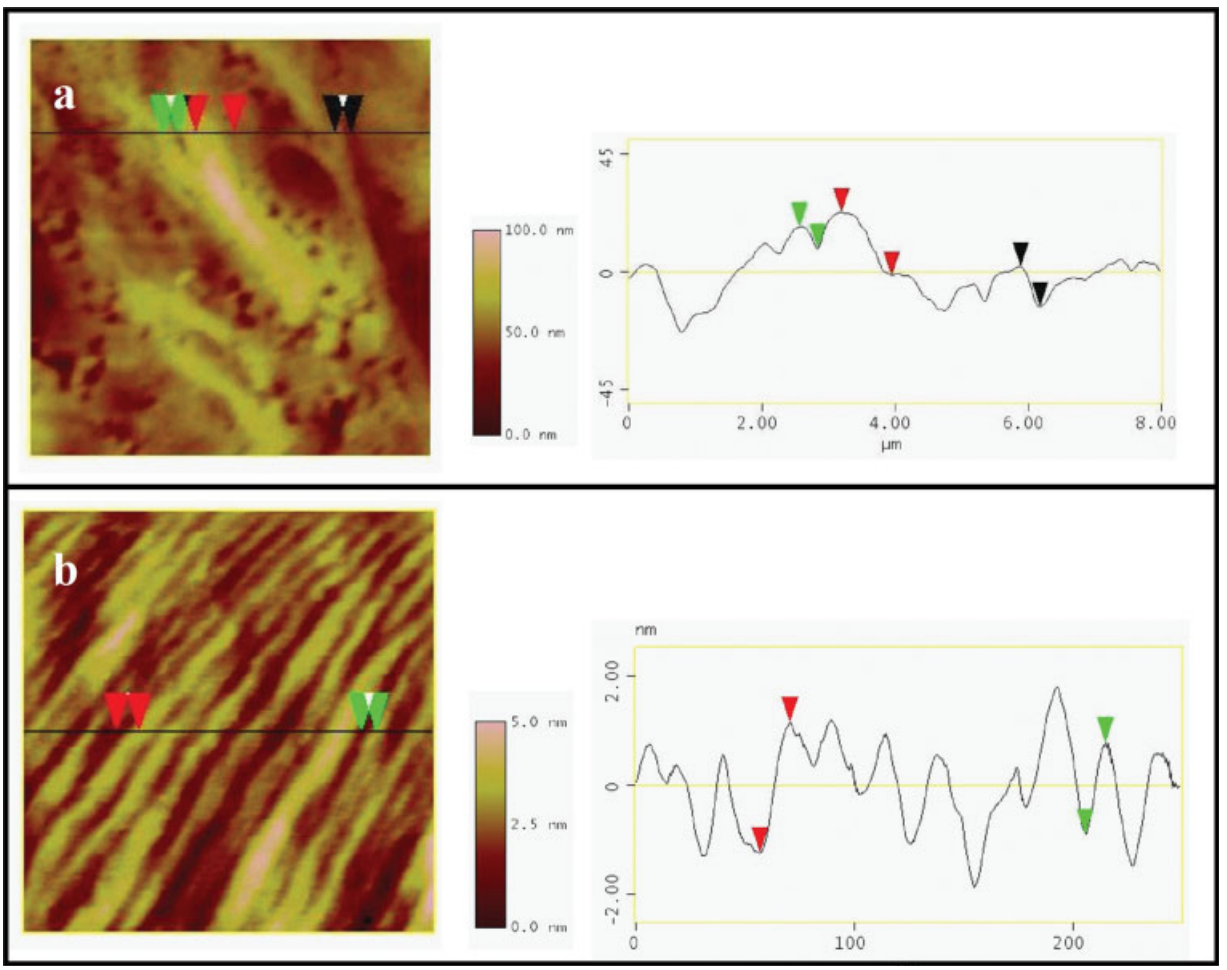

Figure 12 AFM tapping mode height images (top view) and accompanying cross sections showing the lamellar thicknesses of spherulites of (a) pure PHB and (b) PHB/1 wt % xGnP. [Color figure can be viewed in the online issue, which is available at www.interscience.wiley.com.]

ture was also observable in the PHB/1 wt % xGnP-1 system at small scan sizes (250 × 250 nm^2) [Fig. 12(b)], and the thickness was measured to be ~ 5 nm. On the other hand, AFM images of PHB/3 wt % xGnP-1 samples revealed an apparent disruption of the lamellar structure, attributed to the wide distribution of xGnP-1 throughout the crystalline structure (Fig. 13). Overall, these results indicate that the lamellar thickness decreased as the amount of xGnP-1 increased, and was proportional to the size of the crystalline structures formed. These experimental results are consistent with theoretical values for lamellar thicknesses, calculated using the following eq. (6), which relates lamellar thickness to the equilibrium melting temperature of polymers:[27]

$$T_m = T_m^0\left(1 - \frac{2\sigma_e}{\Delta H l}\right), \tag{6}$$

where T_m is the observed melting point, σ_e is the fold surface free energy, ΔH is the heat of fusion, and l is the lamellar thickness. Using this correlation

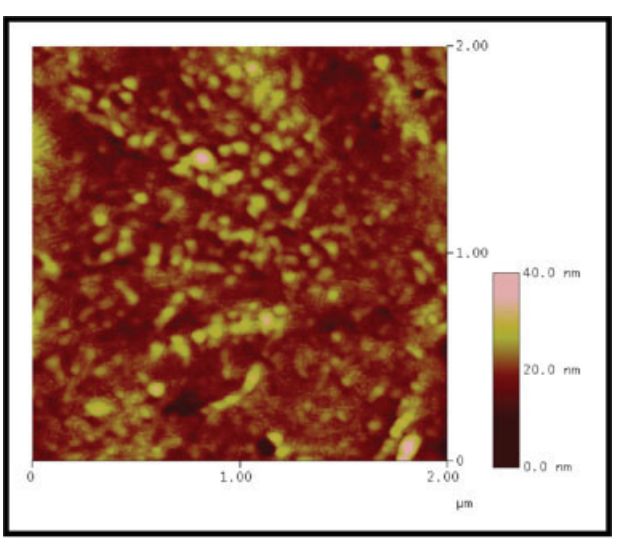

Figure 13 AFM height image (top view) of PHB/3% xGnP-1 showing the apparent disruption of the lamellar structure of the polymer. [Color figure can be viewed in the online issue, which is available at www.interscience.wiley.com.]

and the values reported for σ_e and ΔH ($38 \pm 6 \times 10^{-3}$ J/m^2 and 1.85×10^8 J/m^3, respectively),[27] the lamellar thickness was estimated to be in the range of 17–24 nm. Since the addition of xGnP-1 greatly increases the heterogeneous nucleation ability of PHB, and hence the fold surface energy of the PHB/xGnP-1 composite is expected to differ from pure PHB, the theoretical estimation was not applied for PHB/xGnP-1 systems.

AFM was also employed by Skyes et al.[60] and Murase and coworkers,[61] who used this technique to investigate solution-grown PHB single crystals prepared from bacterial PHB by alkali hydrolysis, and reported the lamellar thickness to be $\sim$ 5 nm.

CONCLUSIONS

This research has shown that exfoliated graphite nanoplatelets efficiently nucleate PHB, leading to systems that crystallize from the melt faster and at higher temperatures. This thermal behavior is particularly desirable for dynamic processing conditions such as extrusion and injection molding, which are largely utilized for obtaining biocomposites. Very small amounts of xGnP-1 (0.01 wt %) increased the crystallization temperature of PHB by $\sim 30^\circ$C, leading to the formation of smaller spherulites, as evidenced by optical microscopy and atomic force microscopy. A modified form of Avrami equation accurately described the nonisothermal crystallization from melt of PHB/xGnP-1 systems, and showed that this process occurred faster for PHB/xGnP-1 systems than for pure PHB. The pure polymer crystallized faster as the cooling rate increased, while the rates of crystallization for the PHB/xGnP-1 systems from the melt were almost independent of the cooling rate. Additionally, nonisothermal crystallization from the melt was shown to be more energetically favored for the systems containing xGnP than for pure PHB. Maximum crystallinity was also achieved faster in PHB/xGnP-1 systems than in pure PHB. Although, the kinetic analysis and activation energies indicate that 3 wt % xGnP in PHB is excessive for initiating nucleation, it should be noted that the excess xGnP may act as a nanoreinforcement, thereby leading to enhanced mechanical properties and possibly achieving electrical conductivity in the bionanocomposites through percolation of the xGnP network.

The effects of xGnP on the crystallization behavior and morphology of PHB provide a foundation for additional investigations of the PHB/xGnP systems with controllable thermal and mechanical properties, and electrical conductivity. Investigations of the mechanical properties of these PHB/xGnP-1 nanocomposites are the focus of ongoing research and these preliminary results indicate improvements in impact and flexural properties compared to the neat polymer.

The authors thank Metabolix Inc. (Cambridge, MA) for providing the poly(hydroxybutyrate) used in this research.

References

1. US_EPA. In United States Environmental Protection Agency's Municipal Solid Waste Factbook; US EPA: Washington, DC, 2006. Available at: http://www.epa.gov/epaoswer/non-hw/muncpl/index.htm
2. US_EPA. In United States Environmental Protection Agency's Municipal Solid Waste Factbook; US EPA, Washington, DC, 2006. Available at http://www.epa.gov/epaoswer/non-hw/muncpl/recycle.htm
3. NFESC. In Joint Services Pollution Prevention Opportunity Handbook; NFESC: Port Hueneme, California, 2005. Available at: http://p2library.nfesc.navy.mil/P2_Opportunity_Handbook/7_I_A_7.html
4. Anastas, P. T.; Warner, J. C. Green Chemistry: Theory and Practice, Oxford University Press: New York, 1998.
5. Dorgan, J. R. L.; Palade, H. J.; Cicero, L. I. Macromol Symp 2001, 175, 55.
6. Tokiwa, Y.; Calabia, B. P. Biotechnol Lett 2004, 26, 1181.
7. Lenz, R. W.; Marchessault, R. H. Biomacromolecules 2005, 6, 1.
8. Doi, Y. Microbial Polyesters; VCH: New York, 1990.
9. Anderson, A. J.; Dawes, E. A. Microbiol Rev 1990, 54, 450.
10. Lundgren, D. G.; Alper, R.; Schnaitm, C., Marchess, Rh. J Bacteriol 1965, 89, 245.
11. Chen, G.-Q. In Biodegradable Polymers for Industrial Applications; Smith, R. Ed.; Woodhead: Cambridge, 2005; pp 32–50.
12. Satkowski, M. M.; Melik, D. H.; Autran, J.-P.; Green, P. R.; Noda, I.; Schechtman, L. A. In Biopolymers, Vol. 3b: Polyesters II — Properties and Chemical Synthesis; Steinbüchel, A.; Doi, Y., Eds.; Wiley-VCH: Weinheim, Chichester, 2001, p 231.
13. Gordeyev, S. A.; Nekrasov, Y. P. J Mater Sci Lett 1999, 18, 1691.
14. Gordeyev, S. A.; Nekrasov, Y. P.; Shilton, S. J. J Appl Polym Sci 2001, 81, 2260.
15. Briassoulis, D. J Polym Environ 2004, 12, 65.
16. Bin, F.; Cheng, C.; Hang, W.; Peng, S. W.; Wang, X. Y.; Dong, L. S.; Xin, J. H. Polymer 2004, 45, 6275.
17. Sato, H.; Padermshoke, A.; Nakamura, M.; Murakami, R.; Hirose, F.; Senda, K.; Terauchi, H.; Ekgasit, S.; Noda, I.; Ozaki, Y. Macromol Symp 2005, 220, 123.
18. Saad, G. R. Polym Int 2002, 51, 338.
19. Chan, C. H.; Kummerlowe, C.; Kammer, H. W. Macromol Chem Phys 2004, 205, 664.
20. Avella, M.; Rota, G. L.; Martuscelli, E.; Raimo, M.; Sadocco, P.; Elegir, G.; Riva, R. J Mater Sci 2000, 35, 829.
21. Abou-Aiad, T. H.; El-Sabee, M. Z.; Abd-El-Nour, K. N.; Saad, G. R.; El-Sayed, E. S. A.; Gaafar, E. A. J Appl Polym Sci 2002, 86, 2363.
22. Wang, X.; Peng, D. L. Colloid Polym Sci 2005 284, 160.
23. Yoshie, N.; Asaka, A.; Inoue, Y. Macromolecules 2004, 37, 3770.
24. Kunze, C.; Freier, T.; Kramer, S.; Schmitz, K. P. J Mater Sci: Mater Med 2002, 13, 1051.
25. Dekoning, G. J. M.; Lemstra, P. J. Polymer 1993, 34, 4089.
26. Dekoning, G. J. M.; Scheeren, A. H. C.; Lemstra, P. J.; Peeters, M.; Reynaers, H. Polymer 1994, 35, 4598.
27. Barham, P. J.; Keller, A.; Otun, E. L.; Holmes, P. A. J Mater Sci 1984, 19, 2781.
28. El-Hadi, A.; Schnabel, R.; Straube, E.; Muller, G.; Henning, S. Polym Test 2002, 21, 665.
29. An, Y. X.; Dong, L. S.; Mo, Z. S.; Liu, T. X.; Feng, Z. L. J Polym Sci Part B: Polym Phys 1998, 36, 1305.
30. He, Y.; Inoue, Y. J Polym Sci Part B: Polym Phys 2004, 42, 3461.

31. Kai, W. H.; He, Y.; Inoue, Y. Polym Int 2005, 54, 780.
32. Liu, W. J.; Yang, H. L.; Wang, Z. Dong, L. S.; Liu, J. J. J Appl Polym Sci 2002, 86, 2145.
33. Withey, R. E.; Hay, J. N. Polymer 1999, 40, 5147.
34. Black, S. N.; Dobbs, B.; Dempsey, P. S.; Davey, R. J. J Mater Sci Lett 1990, 9, 51.
35. Kai, W. H.; He, Y.; Asakaw, N.; Inoue, Y. J Appl Polym Sci 2004, 94, 2466.
36. Barham, P. J. J Mater Sci 1984, 19, 3826.
37. Krishnamoorti, R.; Vaia, R. A.; Giannelis, E. P. Chem Mater 1996, 8, 1728.
38. Park, H. M.; Liang, X. M.; Mohanty, A. K.; Misra, M.; Drzal, L. T. Macromolecules 2004, 37, 9076.
39. Maiti, P.; Batt, C. A.; Giannelis, E. P. Abstr Paper Am Chem Soc 2003, 225, U665.
40. Chen, G. X.; Hao, G. J.; Guo, T. Y.; Song, M. D.; Zhang, B. H. J Appl Polym Sci 2004, 93, 655.
41. Grady, B. P.; Pompeo, F.; Shambaugh, R. L.; Resasco, D. E. J Phys Chem B 2002, 106, 5852.
42. Lai, M. D.; Li, J.; Yang J.; Liu, J. J.; Tong, X.; Cheng, H. M. Polym Int 2004, 53, 1479.
43. Fukushima. H. Chemical Engineering and Materials Science; Michigan State University: East Lansing, MI, 2003.
44. Ruoff, S. R.; Ding, W.; Piner, R.; Stankovich, S. Polym Mater Sci Eng 2005, 92, 511.
45. Liu, T. X.; Mo, Z. S.; Wang, S. G.; Zhang, H. F. Polym Eng Sci 1997, 37, 568.
46. Kong, X. H.; Yang, X. N.; Zhou, E.; Ma, D. Z. Eur Polym J 2000, 36, 1085.
47. Kim, J. Y.; Park, H. S.; Kim, S. H. Polym Mat Sci Eng 2005, 92, 478.
48. Ichikawa, M.; Nakamura, K.; Yoshie, N.; Asakawa, N.; Inoue, Y.; Doi, Y. Macromol Chem Phys 1996, 197, 2467.
49. Hobbs, J. K.; Binger, D. R.; Keller, A.; Barham, P. J. J Polym Sci Part B: Polym Phys 2000, 38, 1575.
50. Gazzano, M.; Focarete, M. L.; Riekel, C.; Scandola, M. Biomacromolecules 2000, 1, 604.
51. Hobbs, J. K.; Winkel, A. K.; McMaster, T. J.; Humphris, A. D. L.; Baker, A. A.; Blakely, S.; Aissaoui, M.; Miles, M. J. Macromol Symp 2001, 167, 1.
52. Binnig, G.; Rohrer, H. Rev Mod Phys 1999, 71, S324.
53. Quate, C. F. Phys Today 1986, 39, 26.
54. Cho, D.; Lee, S.; Yang, G. M.; Fukushima, H.; Drzal, L. T. Macromol Mater Eng 2005, 290, 179.
55. Avrami, M. J Chem Phys 1939, 7, 1103.
56. Avrami, M. J Chem Phys 1939, 8, 212.
57. Liu, T. X.; Moand, Z. S.; Zhang, H. F. J Appl Polym Sci 1998, 67, 815.
58. Jeziorny, A. Polymer 1978, 19, 1142.
59. Kissinger, H. E. J Res Natl Bur Stand 1956, 57, 217.
60. Sykes, K. E.; McMaster, T. J.; Miles, M. J.; Barker, P. A. Barham, P. J.; Seebach, D.; Muller, H. M.; Lengweiler, U. D. J Mater Sci 1995, 30, 623.
61. Murase, T.; Iwata, T.; Doi, Y. Macromol Biosci 2001, 1, 275.